CHEMISTRY OF MATERIALS
Article

Chem. Mater. **2009,** *21,* 4299–4304 4299
DOI:10.1021/cm9015673

Growth Kinetics of Monodisperse Cu−In−S Nanocrystals Using a Dialkyl Disulfide Sulfur Source

Michelle E. Norako, Matthew A. Franzman, and Richard L. Brutchey*

Department of Chemistry and the Center for Energy Nanoscience and Technology, University of Southern California, Los Angeles, California 90089

Received June 6, 2009. Revised Manuscript Received July 31, 2009

Well-defined and monodisperse wurtzite Cu−In−S nanocrystals were synthesized via a solution-based method using di-*tert*-butyl disulfide as the sulfur source. Reaction control (i.e., coordinating solvent, capping ligand, and sulfur source) proved critical for providing a kinetic pathway to the metastable wurtzite phase. The crystal phase was confirmed by powder X-ray diffraction and selected area electron diffraction. Quantitative nanocrystal growth kinetics were studied on a Cu−In−S system for the first time, clearly showing that the nanocrystals pass through a size focusing event before undergoing steady-state Ostwald ripening at later stages of growth. The size-focused 6.9 nm Cu−In−S nanocrystals have an optical band gap of $E_g = 1.47$ eV and an electrochemical band gap of $E_g = 1.84$ eV.

Introduction

There is a growing need for highly efficient, low cost, and elementally nontoxic components for photovoltaic devices, which continues to drive new research in the development of inorganic semiconductor nanocrystals.[1] Solution routes to semiconductor nanocrystals are particularly appealing because they are less energy intensive than vacuum techniques and have the potential for scalability; the nanocrystal suspensions can also be easily deposited via spin-coating or printing.[2] During recent years, there has been significant interest in the development of solution-phase routes to I−III−VI semiconductor nanocrystals, such as $CuInS_2$, $CuInSe_2$, $CuIn_xGa_{1-x}Se_2$.[3−5] This family of semiconductors has band gaps that match well with the solar spectrum, and they can be further tuned by adjusting their relative elemental compositions.[6,7] Of these materials, copper indium sulfide ($CuInS_2$) is particularly attractive because it possesses a direct band gap ($E_g \approx 1.45-1.50$ eV), has a large absorption coefficient and good photostability, has exhibited power conversion efficiencies of 12% in photovoltaic devices, and avoids heavy elements such as selenium.[8−11] Nanocrystals of $CuInS_2$ have been previously synthesized by heating copper and indium salts with a sulfur source (e.g., dithiocarbamates,[6,12] thiourea,[13,14] thiols,[15,16] elemental sulfur,[7,17] and carbon disulfide[18]) at temperatures ranging between 180 and 250 °C, which typically yields the thermodynamically stable tetragonal chalcopyrite phase.[6,7,15,17,18]

Very recently, $CuInS_2$ nanocrystals were found to also adopt a hexagonal wurtzite (wz) phase, which was first observed by Lu and co-workers.[12] In the bulk, wz-$CuInS_2$ is a high-temperature phase stable between 1045 and 1090 °C, in which the copper and indium cations randomly share common lattice sites.[19] As such, the wurtzite phase of $CuInS_2$ allows for a high degree of compositional variability, resulting in stable, nonstoichiometric Cu−In−S nanocrystals. Observation of wz−Cu−In−S nanocrystals at room temperature proves that the metastable phase is kinetically accessible under less energy

*Corresponding author.

(1) Greenham, N. C.; Peng, X. G.; Alivisatos, A. P. *Phys. Rev. B* **1996**, *54*, 17628.
(2) Sargent, E. H. *Nat. Photonics* **2009**, *3*, 325.
(3) Tang, J.; Hinds, S.; Kelley, S. O.; Sargent, E. H. *Chem. Mater.* **2008**, *20*, 6906.
(4) Koo, B.; Patel, R. N.; Korgel, B. A. *J. Am. Chem. Soc.* **2009**, *131*, 3134.
(5) Guo, Q.; Kim, S. J.; Kar, M.; Shafarman, W. N.; Birkmire, R. W.; Stach, E. A.; Agrawal, R.; Hillhouse, H. W. *Nano Lett.* **2008**, *8*, 2982.
(6) Pan, D.; Wang, X.; Zhou, Z. H.; Chen, W.; Xu, C.; Lu, Y. *Chem. Mater.* **2009**, *21*, 2489.
(7) Xie, R.; Rutherford, M.; Peng, X. *J. Am. Chem. Soc.* **2009**, *131*, 5691.
(8) Yoshino, K.; Ikari, T.; Shirakata, S.; Miyake, H.; Hiramatsu, K. *Appl. Phys. Lett.* **2001**, *78*, 742.
(9) Braunger, D.; Hariskos, D.; Walter, T.; Schock, H. W. *Sol. Energy Mater. Sol Cells* **1996**, *40*, 97.
(10) Klenk, R.; Blieske, U.; Dieterle, V.; Ellmer, K.; Fiechter, S.; Hengel, I.; Jager-Waldau, A.; Kampschulte, T.; Kaufmann, C.; Klaer, J.; Lux-Steiner, M. C.; Braunger, D.; Hariskos, D.; Ruckh, M.; Schock, H. W. *Sol. Energy Mater. Sol Cells* **1997**, *49*, 349.
(11) Alonso, M. I.; Wakita, K.; Pascual, J.; Garriga, M.; Yamamoto, N. *Phys. Rev. B* **2001**, *63*, 75203.
(12) Pan, D.; An, L.; Sun, Z.; Hou, W.; Yang, Z.; Lu, Y. *J. Am. Chem. Soc.* **2008**, *130*, 5620.
(13) Qi, Y.; Liu, Q.; Tang, K.; Liang, Z.; Ren, Z.; Liu, X. *J. Phys. Chem. C* **2009**, *113*, 3939.
(14) Koo, B.; Patel, R. N.; Korgel, B. A. *Chem. Mater.* **2009**, *21*, 1962.
(15) Zhong, H.; Zhou, Y.; Ye, M.; He, Y.; Ye, J.; He, C.; Yang, C.; Li, Y. *Chem. Mater.* **2008**, *20*, 6434.
(16) Connor, S. T.; Hsu, C.-M.; Weil, B. D.; Aloni, S.; Cui, Y. *J. Am. Chem. Soc.* **2009**, *131*, 4962.
(17) Panthani, M. G.; Akhavan, V.; Goodfellow, B.; Schmidtke, J. P.; Dunn, L.; Dodabalapur, A.; Barbara, P. F.; Korgel, B. A. *J. Am. Chem. Soc.* **2008**, *130*, 16770.
(18) Du, W.; Qian, X.; Yin, J.; Gong, Q. *Chem.—Eur. J.* **2007**, *13*, 8840.
(19) Binsma, J. J. M.; Giling, L. J.; Bloem, J. *J. Cryst. Growth* **1980**, *50*, 429.

Published on Web 08/18/2009

intensive conditions,[12−14,16,20] and offers the potential of discovering new optoelectronic and morphological properties specific to this crystal phase.

The synthesis of chalcopyrite and wurtzite Cu−In−S nanocrystals continues to be an area of active research, in which various reaction conditions and precursors have been used to obtain nanocrystals with varying degrees of size and shape control. As part of an ongoing investigation into using dialkyl dichalcogenides as low temperature chalcogen sources,[21−23] we report the rational synthesis of very well-defined, monodisperse wz−Cu−In−S nanocrystals using di-*tert*-butyl disulfide as the sulfur source. Only by exerting specific reaction control (i.e., coordinating solvent, disulfide sulfur source, capping ligand) is the synthesis of monodisperse wz−Cu−In−S nanocrystals made possible. Because the optoelectronic properties of semiconductor nanocrystals are highly dependent on their size and distribution of size, we have also studied the quantitative growth kinetics of Cu−In−S nanocrystals for the first time and found that they undergo a size focusing event, which is highly dependent upon the identity of capping ligands present in solution.

Experimental Details

General Considerations. Copper(I) chloride (CuCl, Strem Chemicals, 99.999%), indium(III) acetylacetonate ($In(acac)_3$, Strem Chemicals, 98%), oleylamine (*cis*-9-octadecenylamine, Aldrich, 70%), 1-dodecanethiol (Alfa Aesar, 98%), di-*tert*-butyl disulfide (Chem Service, 99.3%), precipitated sulfur powder (Alfar Aesar, 99.5%), *tert*-butyl mercaptan (TCI America, 98%), and squalane (Alfa Aesar, 98%) were all purchased and used without further purification. Nanocrystal syntheses were performed under nitrogen, in the absence of water and oxygen, using standard Schlenk techniques.

Cu−In−S Nanocrystal Synthesis. In a typical synthesis, $In(acac)_3$ (0.30 g, 0.71 mmol) and CuCl (0.071 g, 0.71 mmol) were added to a two-neck round-bottom flask fitted with a reflux condenser and rubber septum. Oleylamine (2.32 g, 8.67 mmol) and 1-dodecanethiol (0.34 mL, 1.4 mmol) were added to a Schlenk flask and were cycled between vacuum and nitrogen three times. The oleylamine/1-dodecanethiol mixture was then transferred to the reaction flask containing the metal salts via cannula. Prior to heating, the system was cycled between vacuum and nitrogen three times, heated (10 °C min^{-1}) to 95 °C, and again cycled three times between vacuum and nitrogen to eliminate adventitious water and dissolved oxygen. Di-*tert*-butyl disulfide (0.40 mL, 2.1 mmol) was quickly injected into the system under flowing nitrogen, and the temperature was increased (10 °C min^{-1}) to 180 °C and allowed to react for 33 min with stirring. After being cooled to room temperature, the reaction mixture was dissolved in 2 mL of dichloromethane, sonicated, and centrifuged (6000 rpm for 15 min) to yield a black solid. Precipitation was repeated with toluene (0.5 mL) and ethanol (10 mL) to yield the purified product. The resulting Cu−In−S nanocrystals form suspensions in organic solvents such as hexane and toluene that are stable for several weeks.

Instrumentation. Powder X-ray diffraction (XRD) analyses were performed on a Rigaku Ultima IV X-ray diffractometer using a Cu Kα radiation source ($\lambda = 1.54$ Å). Transmission electron microscopy (TEM) and selected area electron diffraction (SAED) were performed on a JEOL JEM-2100 microscope at an operating voltage of 200 kV, equipped with a Gatan Orius CCD camera. SAED patterns were collected at a camera distance of 60 cm. Energy dispersive X-ray spectroscopy (EDX) was performed on an EDAX Apollo silicon drift detector (SDD) attached to a JEOL JSM-6610 scanning electron microscope operating at 20 keV. Samples were deposited on an aluminum tab and 10 areas were randomly analyzed. UV−vis−NIR spectra were acquired on a Cary 14 spectrophotometer in dual beam mode using quartz cuvettes with 1 cm path lengths from nanocrystal suspensions in cyclohexane. Cyclic voltammetry (CV) curves were acquired on a Princeton Applied Research Potentiostat/Galvometer Model 283. The tetra-*n*-butylammonium hexafluorophosphate ($TBAPF_6$, Alfa-Aesar, 98%) electrolyte (0.3 M in dry, deoxygenated acetonitrile) was added to a dry three-neck round-bottom flask equipped with three rubber septa. Glassy carbon, Pt, and Ag/Ag^+ electrodes were inserted into the solution via the rubber septa and served as the working, counter, and reference electrodes, respectively. A 0.1 mL toluene suspension of the nanocrystals (30−40 mg/mL) mixed with the electrolyte (~1.0 mg) was added dropwise to the surface of the carbon electrode to form a thin black film that adheres to the surface when submerged in the acetonitrile. CV curves were acquired under an inert atmosphere at a scan rate of 10 mV s^{-1}. The HOMO and LUMO energy levels were calculated from the oxidation potential (E'_{ox}) and reduction potential (E'_{red}), respectively, according to

$$E_{HOMO} = -I_p = -(E'_{ox} + 4.71)\ \text{eV}$$

$$E_{LUMO} = -E_a = -(E'_{red} + 4.71)\ \text{eV}$$

where potential values are relative to the Ag/Ag^+ reference electrode.

TEM Analysis of Nanocrystal Growth. Aliquots (0.10−0.25 mL) of the reaction mixture were taken by syringe at specified times and quenched via cooling to room temperature. Nanocrystals were precipitated from the reaction mixture as described above and dissolved in toluene. TEM samples were prepared on 300 mesh carbon-coated copper grids (Ted Pella, Inc.). Each data point in the statistical analysis represents more than 350 particles.

Results and Discussion

Nanocrystal Synthesis and Characterization. Nanocrystals of Cu−In−S were synthesized via the fast addition of di-*tert*-butyl disulfide into a mixture of CuCl, $In(acac)_3$, oleylamine, and 1-dodecanethiol, which was then heated to 180 °C. The resulting 0D nanocrystals are monodisperse with a mean diameter of 6.9 ± 0.6 nm, as determined by TEM analysis (Figure 1). Rather than the thermodynamically preferred chalcopyrite phase, XRD analysis revealed that the nanocrystals are composed of wz−Cu−In−S with no evidence of crystalline Cu_2S or In_2S_3 impurities (Figure 2). The lattice constants of $a = 3.9 \pm 0.1$ Å and $c = 6.4 \pm 0.1$ Å calculated for the

(20) Nose, K.; Soma, Y.; Omata, T.; Otsuka-Yao-Matsuo, S. *Chem. Mater.* **2009**, *21*, 2607.
(21) Franzman, M. A.; Perez, V.; Brutchey, R. L. *J. Phys. Chem. C* **2009**, *113*, 630.
(22) Franzman, M. A.; Brutchey, R. L. *Chem. Mater.* **2009**, *21*, 1790.
(23) Webber, D. H.; Brutchey, R. L. *Chem. Commun.* **2009** No. DOI:10.1039/ B912434A.

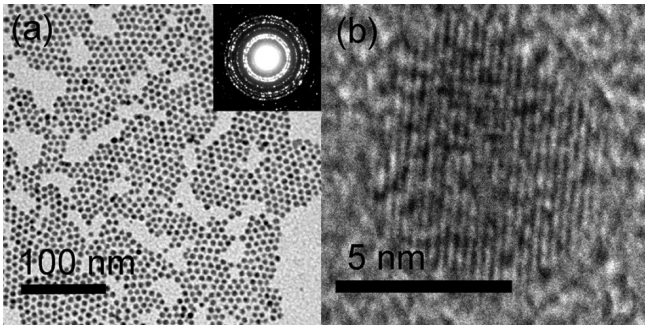

Figure 1. (a) TEM micrograph of 6.9 nm Cu−In−S nanocrystals with representative SAED pattern displayed as inset. (b) HRTEM micrograph of an individual Cu−In−S nanocrystal.

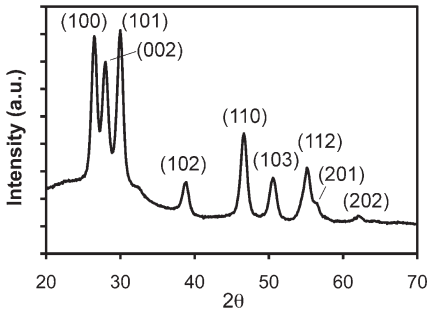

Figure 2. XRD pattern of the wurtzite Cu−In−S nanocrystals synthesized with di-*tert*-butyl disulfide in oleylamine at 180 °C.

nanocrystals are in good agreement with the values reported by Lu and others (a = 3.9 Å and c = 6.4 Å).[12] The size of the nanocrystals estimated by the Scherrer formula was 8.4 ± 0.3 nm, which is in close agreement with the TEM data.

High-resolution TEM (HRTEM) and SAED analysis of individual Cu−In−S nanocrystals is consistent with the wurtzite phase. An HRTEM image of an individual nanocrystal with the wurtzite-specific (102) lattice planes displayed (d = 0.25 nm) is shown in Figure 1b. Moreover, the lattice constants from randomly selected SAED patterns (Figure 1 inset) agree with those calculated from the XRD results for wz−Cu−In−S. Because the relative elemental composition of wz−Cu−In−S can vary greatly, the nanocrystals were analyzed by EDX. Analysis of ten randomly selected areas gave an average Cu:In:S composition of 0.51:0.11:0.38, which is compositionally quite different from the expected 0.25:0.25:0.50 stoichiometry for $CuInS_2$. Because copper and indium share lattice sites in the wurtzite structure, this $Cu_{4.6}In_{1.0}S_{3.5}$ composition still falls within the phase space for wz−Cu−In−S.[19] Also, no other crystal phases were observed by SAED analysis of randomly selected areas.

It was found that the particular reagents employed for this synthesis play a decisive role in the formation of wz−Cu−In−S. In a result similar to those of Tang and Omata,[13,20] it was observed that substituting an equal volume of squalane (i.e., a noncoordinating solvent) for oleylamine under otherwise identical conditions produced the tetragonal chalcopyrite phase of Cu−In−S (see the Supporting Information, Figure S1). This suggests that the coordination of oleylamine to the metal cations likely has a kinetic influence on phase determination. The choice of sulfur source also plays a critical role in the formation of monodisperse wz−Cu−In−S nanocrystals. Di-*tert*-butyl disulfide was chosen as the sulfur source because (i) it is a liquid that is soluble in common organic solvents, and (ii) it possesses a relatively weak S−S bond that should aid in relatively low temperature decomposition and sulfur transfer. Di-*tert*-butyl disulfide is known to thermally decompose in the gas phase to give isobutylene, hydrogen sulfide, and a small amount of elemental sulfur.[24] Under the synthesis conditions, the disulfide is activated in solution to release sulfur species which can then react with the metal cations. As described previously for the synthesis of In_2S_3 nanorods with di-*tert*-butyl disulfide, metal sulfide formation is relatively slow at 180 °C,[22] which may be key in phase determination in the wz−Cu−In−S system.

Elemental sulfur can serve as an effective sulfur source to create a variety of metal sulfide nanocrystals;[25] however, sulfur is poorly soluble in most solvents at modest reaction temperatures. When elemental sulfur was used in place of di-*tert*-butyl disulfide (equimolar based on sulfur atoms), no crystalline product was observed under otherwise identical conditions. When an equimolar amount of *tert*-butyl mercaptan is used (per sulfur atom) as the sole sulfur source, the phase impure tetragonal chalcopyrite Cu−In−S is observed (see the Supporting Information, Figure S2). It is well-known that thiols can act as sulfur sources for the formation of metal sulfide nanocrystals;[26,27] however, the decomposition and sulfur transfer rates of the disulfide and mercaptan are sufficiently different in order to exert a kinetic influence on phase determination. The effect of adjusting the molar ratio of oleylamine to 1-dodecanethiol was also investigated. Results indicate that when molar ratios are between 14:0 and 12:2 oleylamine/1-dodecanethiol, nanocrystals in the wurtzite phase are formed. Higher concentrations of 1-dodecanethiol (e.g., 10:4 oleylamine/1-dodecanethiol) resulted in no nanocrystalline product being formed. Preference for the wurtzite phase over the chalcopyrite phase is not a direct result of any one component in this system; rather, it is a combination of kinetic variables that leads to phase determination. The decomposition rate of the disulfide, the presence of coordinating solvents such as oleylamine, reaction temperature, and concentration of metal cations in solution combine to form the proper environment for the selective formation of metastable wz−Cu−In−S nanocrystals.

Nanocrystal Growth Kinetics. There have been significant advances in the synthesis of I−III−VI semiconductor nanocrystals; however, there have been no quantitative reports on the growth kinetics of these nanocrystals in solution. Understanding the growth

(24) Bock, H.; Mohmand, S. *Angew. Chem., Int. Ed.* **1977**, *16*, 104.
(25) Liu, J.; Yu, H.; Wu, Z.; Wang, W.; Peng, J.; Cao, Y. *Nanotechnology* **2008**, *17*, 345602.
(26) Choi, S. H.; Kim, E. G.; Hyeon, T. *J. Am. Chem. Soc.* **2006**, *128*, 2520.
(27) Han, W.; Yi, L.; Zhao, N.; Tang, A.; Gao, M.; Tang, Z. *J. Am. Chem. Soc.* **2008**, *130*, 13152.

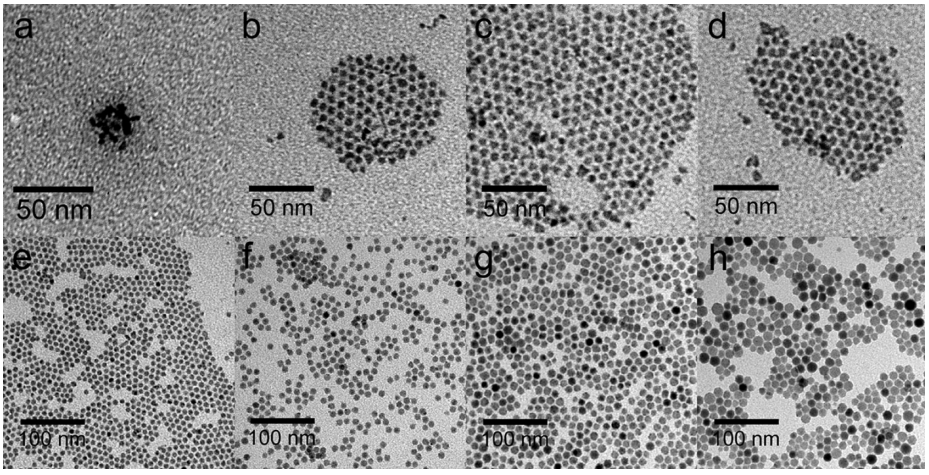

Figure 3. Representative TEM micrographs demonstrating the temporal evolution of the size and size distribution of Cu−In−S nanocrystals taken from the reaction mixture at t = (a) 1, (b) 18, (c) 23, (d) 28, (e) 33, (f) 68, (g) 128, and (h) 188 min.

kinetics, as well as developing a rational synthetic methodology, will ensure greater control over nanocrystal size and shape. To investigate the growth kinetics of the Cu−In−S nanocrystals, we took aliquots throughout the course of the reaction and the corresponding TEM images were statistically analyzed, thus creating a quantitative view of Cu−In−S nanocrystal growth. Representative TEM images from each sample are shown in Figure 3 and the corresponding statistical data is displayed in Figure 4.

Nanocrystal nucleation was observed visually when the reaction solution rapidly changed from yellow to black after several seconds of heating at 180 °C. Nanocrystals large enough to be observed by TEM form 1 min after nucleation. As demonstrated in Figure 3a, these primitive nanocrystals are small (3.7 ± 0.9 nm), ill defined in regard to shape, and agglomerated. Growth is sustained during the initial stage, eventually producing nanocrystals that are 6.9 nm in diameter (Figure 3e) after t = 33 min. From the initial nucleation event, the nanocrystals size focus until this point in time where the size distribution, as represented by standard deviation about the mean, reaches a minimum of σ_D/μ_D = 9.1% (Figure 4b). Such size focusing growth kinetics have been previously observed in the synthesis of monodisperse manganese oxide and iron oxide nanocrystals.[28,29] After this invariant region at t = 33 min, the standard deviation of the Cu−In−S nanocrystals begins to gradually increase, with the standard deviation about the mean increasing from σ_D/μ_D = 9.1 to 31.4% (Figure 4b). In addition, after t = 33 min, the nanocrystals begin to grow at a slower linear rate, which suggests a steady-state Ostwald ripening mechanism (Figure 4a).[30] At this stage of growth, smaller nanocrystals are absorbed by larger nanocrystals, causing the Cu−In−S nanocrystal population to evolve into an more polydispersed ensemble as time progresses.

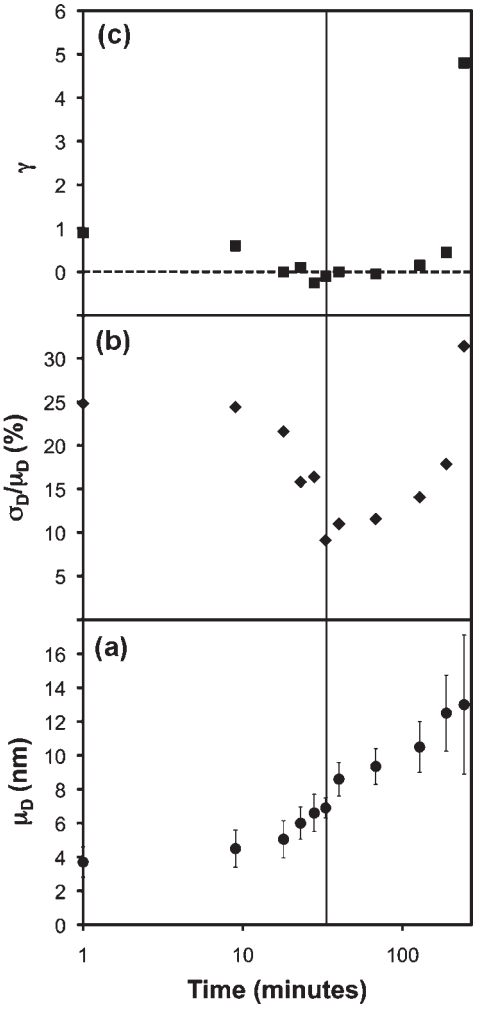

Figure 4. Quantitative statistical results for the nanocrystal growth represented in Figure 3. Temporal evolution of the (a) mean diameter (μ_D), (b) distribution about the mean (σ_D/μ_D), and (c) skew (γ) for the Cu−In−S nanocrystals. A vertical line is drawn at t = 33 min.

Closer analysis of the statistical data reveals further evidence of a late Ostwald ripening stage. After t = 33 min, the degree of asymmetry, or skew (γ), steadily shifts toward more positive values. Skew represents a divergence from a normal Gaussian distribution and,

(28) Kwon, S. G.; Piao, Y.; Park, J.; Anappane, S.; Jo, Y.; Huang, N.-M.; Park, J.-G.; Hyeon, T. *J. Am. Chem. Soc.* **2007**, *129*, 12571.
(29) Chen, Y.; Johnson, E.; Peng, X. *J. Am. Chem. Soc.* **2007**, *129*, 10937.
(30) Lifshitz, I. M.; Slyozov, V. V. *J. Phys. Chem. Solids* **1961**, *19*, 35.

along with mean and standard deviation, is one the first three standardized moments of the growing population.[31] A positive skew indicates an increased population of larger particles in the sample population relative to the mean, whereas a negative skew indicates a greater population of smaller particles in the sample population about the mean. During the final 210 min of nanocrystal growth, the population of nanocrystals that are larger than the statistical average increases with time, and the degree of asymmetry reaches more positive values (Figure 4c). Interestingly, after 240 min of heating, there are no particles that are more than double the mean particle size, indicating that the Cu−In−S growth trend matches well with the predications described by Lifshitz et al.[30]

Monitoring the elemental composition during the course of the reaction revealed that the evolving nanocrystals begin as copper-rich (Cu:In:S composition of 0.58:0.11:0.31) and remain so throughout the size-focusing period (vide supra). After 33 min, the nanocrystals slowly become more compositionally stoichiometric during the steady-state Ostwald ripening stage of growth. The concentration of indium and sulfur increase relative to the copper concentration until an average Cu:In:S composition of 0.23:0.27:0.50 is reached at 188 min (see the Supporting Information, Figure S3). The initially high concentration of copper relative to indium and sulfur may be a result of the copper nucleating faster than the indium and sulfur. It has been previously shown by difference FT-IR spectroscopy that $In(acac)_3$ decomposes slowly over the course of ca. 160 min in the presence of oleylamine at 180 °C.[21] Similarly, the reaction between $In(acac)_3$ and di-*tert*-butyl disulfide does not form nanocrystalline β-In_2S_3 until after 420 min in oleylamine at 180 °C, suggesting a similarly slow rate of sulfur transfer.[22] Therefore, the rates of precursor decomposition may influence not only the crystal phase but also the elemental composition of the nanocrystals.

Nanocrystal growth was also monitored by XRD to determine evolution of the nanocrystal phase and size as a function of time. XRD patterns of the nanocrystals isolated from the reaction mixture at $t = 15$ min, 25, 60, and 180 min show a gradual sharpening of the reflections as time progresses, indicating nanocrystal growth (see the Supporting Information, Figure S4). By applying the Scherrer equation, the nanocrystal sizes at $t = 15$ min (5.1 nm), 25 min (6.8 nm), 60 min (9.0 nm), and 180 min (12.8 nm) were shown to corroborate nanocrystal sizes measured directly by TEM analysis. Interestingly, the wurtzite phase is observed through the entire reaction course without passing through any intermediate phases.

The addition of 2 mol equiv of 1-dodeceanethiol relative to copper and indium is critical for the synthesis of monodisperse Cu−In−S nanocrystals. When 1-dodecanethiol is not used in the synthesis, large single-crystalline hexagonal platelets of wz−Cu−In−S are formed after

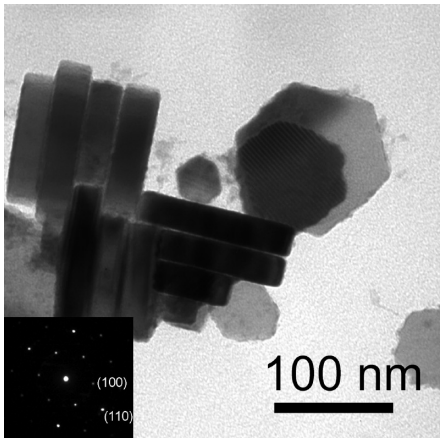

Figure 5. TEM micrograph of wurtzite Cu−In−S hexagonal platelets formed without 1-dodecanethiol, with representative SAED pattern displayed as inset.

180 min (Figure 5) that are polydisperse in diameter (30−130 nm) but uniform in thickness (25.0 ± 1.9 nm). This is compared to the size-controlled Cu−In−S nanocrystals (mean size = 12.5 nm after 180 min) when 1-dodeceanethiol is used during synthesis. XRD analysis confirmed the large hexagonal platelets are also in the wurtzite phase (see the Supporting Information, Figure S5), and EDX gave an average Cu:In:S composition of 0.29:0.24:0.47, which is very close to stoichiometric $CuInS_2$. The ratio of oleylamine/1-dodecanethiol strongly influences the overall phase and morphology of the Cu−In−S nanocrystals (vide supra). In the absence of 1-dodecanethiol, fast nanocrystal growth is observed. This suggests that 1-dodecanethiol binds more strongly than oleylamine to the exposed nanocrystal faces, resulting in an arrested growth condition.

Band Gap Determination. The band gap of the Cu−In−S nanocrystals was determined by UV−vis−NIR spectroscopy and CV. The band gap of bulk chalcopyrite $CuInS_2$ is $E_g \approx 1.45$ eV, with a Bohr radius of 4.0 nm,[15] which suggests that very small nanocrystals are needed to observe significant quantum confinement effects. The as-synthesized 6.9 nm wz−Cu−In−S nanocrystals absorb strongly through the entire visible region of the spectrum resulting in the black color of the material (Figure 6a). The band gap of the 6.9-nm Cu−In−S nanocrystals was approximated from the onset of the absorption spectrum to be $E_g = 1.47$ eV, consistent with the band gap of other chalcopyrite and wurtzite Cu−In−S nanocrystals and close to that of bulk $CuInS_2$.[6,14,16] Cyclic voltammetry can also be used to estimate the band gap for semiconductor nanocrystals.[32] A typical CV curve for the 6.9-nm Cu−In−S nanocrystals deposited as a thin film on the carbon working electrode is given in Figure 6b. Relative to a Ag/Ag^+ reference electrode, the oxidation (E'_{ox}) and reduction (E'_{red}) potentials of the nanocrystals are 1.13 and −0.71 V, respectively. The separation between the E'_{ox} and E'_{red} peaks gives an electrochemical band gap of $E_g = 1.84$ eV and HOMO and LUMO levels of −5.84 and

(31) Peng, X.; Wickham, J.; Alivisatos, A. P. *J. Am. Chem. Soc.* **1998**, *120*, 5343.

(32) Li, Y.; Zhong, H.; Li, R.; Zhou, Y.; Yang, C.; Li, Y. *Adv. Funct. Mater.* **2006**, *16*, 1705.

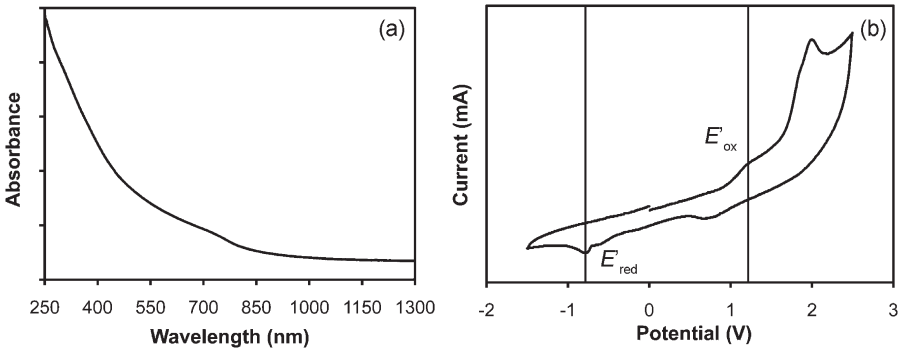

Figure 6. (a) UV−vis absorption spectrum and (b) cyclic voltammetry curve (sweep rate = 10 mV s^{-1}) for the 6.9 nm Cu−In−S nanocrystals.

−4.00 eV, respectively. The electrochemical band gap is greater than the band gap estimated from the absorption spectrum; however, higher electrochemical band gaps have also been observed in the case of II−VI nanocrystals.[32] To confirm that these oxidation and reduction peaks result from the purified nanocrystals, we took CV curves of the blank electrolyte and varying concentrations of 1-dodecanethiol added to the solution (see the Supporting Information, Figure S6). As the concentration of 1-dodecanethiol increases, peaks at ~1.68 and 0.47 V appear, increasing in peak current with increasing concentration. These peaks are attributed to redox processes pertaining to the thiol. Thus, it appears the E'_{ox} and E'_{red} peaks at 1.13 and −0.71 V, respectively, can be assigned to the Cu−In−S nanocrystals. The reduction and oxidation peak assignments correlate well with valence and conduction band energies previously calculated and experimentally determined for the chalcopyrite phase of $CuInS_2$.[33,34]

Conclusion

A facile solution-phase synthesis was developed using di-*tert*-butyl disulfide to produce monodisperse 6.9-nm Cu−In−S nanocrystals in the metastable wurtzite phase. The keys to wz−Cu−In−S formation appear to be coordination of the oleylamine solvent to the metal cation precursors and relatively slow sulfur transfer from the disulfide. It was found that the growth kinetics described above adhere nicely to a model recently proposed by Bawendi and Jensen.[35] From the nucleation event to about $t = 28$ min, a size focusing event (region III in the Bawendi−Jensen model) occurs whereby the mean nanocrystal size increases with a concomitant focusing of the standard deviation about the mean. At $t = 33$ min, a short invariant region (region IV) is observed where the minimum standard deviation about the mean is achieved (i.e., $\sigma_D/\mu_D = 9.1\%$). Following this, the mean nanocrystal size begins to increase again with a simultaneous increase in the standard deviation about the mean (region V). In addition to adhering to this theoretical model, the data are qualitatively similar to the empirical growth kinetics described recently for $(Fe_3O_4)_x$-$(Fe_2O_3)_{1-x}$,[28] MnO,[29] and CdSe[36] nanocrystals. Importantly, it was determined that 1-dodecanethiol was critical for the growth of monodisperse Cu−In−S nanocrystals under these conditions. Taken together, the synthesis of monodisperse wz−Cu−In−S was achieved through reaction control (i.e., choice of solvent, capping ligand, and sulfur source). These nanocrystals were found to have an optical band gap of 1.47 eV that matches well with the solar spectrum. Future work will focus on exerting an extra level of reaction control to make compositional variants of this Cu−In−S system to tune the band gap for potential photovoltaic applications.

Acknowledgment. This material is based on work supported by the National Science Foundation under DMR-0906745. The authors are thankful for the generous support provided by the Department of Chemistry and the College of Letters, Arts & Sciences at USC. Acknowledgement is also made to the Anton Burg Foundation for financial assistance toward the purchase of the XRD. We also thank Prof. M. Thompson for use of his CV apparatus.

Supporting Information Available: XRD patterns and TEM images for various control reactions; XRD of hexagonal platelets of wz−Cu−In−S; EDX spectra and elemental composition vs time; additional CV curves (PDF). This material is available free of charge via the Internet at http://pubs.acs.org.

(33) Jaffe, J. E.; Zunger, A. *Phys. Rev. B* **1983**, *28*, 5822.
(34) Courtel, F. M.; Paynter, R. W.; Marsan, B.; Morin, M. *Chem. Mater.* **2009** No. DOI:10.1021/cm900601k.
(35) Rempel, J. Y.; Bawendi, M. G.; Jensen, K. F. *J. Am. Chem. Soc.* **2009**, *131*, 4479.
(36) Yen, B. K. H.; Stott, N. E.; Jensen, K. F.; Bawendi, M. G. *Adv. Mater.* **2003**, *15*, 1858.